PNAS

Supplementary Information for

The nature of proton-coupled electron transfer in a blue light using flavin domain

Zhongneng Zhou[a,1], Zijing Chen[a,1], Xiu-Wen Kang[a], Yalin Zhou[a], Bingyao Wang[a], Siwei Tang[a], Shuhua Zou[a], Yifei Zhang[a], Qiaoyu Hu[b], Fang Bai[b], Bei Ding[a,*], Dongping Zhong[a,c,*]

[a]Center for Ultrafast Science and Technology, School of Chemistry and Chemical Engineering, Shanghai Jiao Tong University, Shanghai 200240, China; [b]Shanghai Institute for Advanced Immunochemical Studies and School of Life Science and Technology, ShanghaiTech University, Shanghai 201210, China; [c]Department of Physics, Department of Chemistry and Biochemistry, and Programs of Biophysics, Chemical Physics, and Biochemistry, Ohio State University, Columbus, OH 43210.

[*]To whom correspondence may be addressed.

Email: bei.ding@sjtu.edu.cn; zhong.28@osu.edu

This PDF file includes:

Table of Contents

Supplementary Information Text

Experimental

Plasmid Construction and Primers Design

The wild type $OaPAC_{1\text{-}102}$ (referred to as $OaPAC_{BLUF}$) protein expression gene sequence was obtained from GenBank (AFY83176.1) and synthesized by Genewiz. The $OaPAC_{BLUF}$ plasmid was constructed by inserting the protein expression fragment into a pET28a vector at the *Nde*I-*Hin*dIII restriction sites, enabling overexpression in *E. coli* with an amino terminus His tag. The reconstructed plasmid (hereafter referred to as $pETOaPAC_{BLUF}$) was purchased from Genewiz and gene sequencing was conducted to ensure the expression gene sequence is correct.

To investigate the photochemistry of $OaPAC_{BLUF}$, several mutants were designed including W90F, Y6F/W90F, Q48A/W90F, Q48E/W90F. The mutant plasmids were constructed using the QuickMutation site-directed mutagenesis kit (D0206, Beyotime) and $pETOaPAC_{BLUF}$ as a template. The primer sequences used were listed as below and all plasmids constructed were verified by sequencing.

Mutant	Primer Sequences
W90F (referred to as WT)	5'-GTCCAAGAAAGAATGTTTCCTGATTTCTCCATGCAAACGATTAACCTGG-3' 5'-CCAGGTTAATCGTTTGCATGGAGAAATCAGGAAACATTCTTTCTTGGAC-3'
Y6F/W90F	5'-GAAAAGACTCACCTTTATTAGTAAATTTTCCCGCCCCCTC-3' 5'-GAGGGGGCGGGAAAATTTACTAATAAAGGTGAGTCTTTTC-3' 5'-GTCCAAGAAAGAATGTTTCCTGATTTCTCCATGCAAACGATTAACCTGG-3' 5'-CCAGGTTAATCGTTTGCATGGAGAAATCAGGAAACATTCTTTCTTGGAC-3'
Q48A/W90F (referred to as Q48A)	5'-GTCTGGACGGGATATTTTTTGCCATCCTCGAAGGCGAAGCGGAG-3' 5'-CTCCGCTTCGCCTTCGAGGATGGCAAAAAATATCCCGTCCAGAC-3' 5'-GTCCAAGAAAGAATGTTTCCTGATTTCTCCATGCAAACGATTAACCTGG-3' 5'-CCAGGTTAATCGTTTGCATGGAGAAATCAGGAAACATTCTTTCTTGGAC-3'
Q48E/W90F (referred to as Q48E)	5'-CTGGACGGGATATTTTTTGAAATCCTCGAAGGCGAAGCG-3' 5'-CGCTTCGCCTTCGAGGATTTCAAAAAATATCCCGTCCAG-3' 5'-GTCCAAGAAAGAATGTTTCCTGATTTCTCCATGCAAACGATTAACCTGG-3' 5'-CCAGGTTAATCGTTTGCATGGAGAAATCAGGAAACATTCTTTCTTGGAC-3'

Protein Expression and Purification

All of the $OaPAC_{BLUF}$ mutants including the native wild-type were expressed and purified with a standard laboratory method. First, the expression plasmid was transformed into the BL21(DE3) strain of *E. coli*. The transformed cells were grown in LB medium supplemented with kanamycin (50 ug/mL) at 30 ºC to OD_{600} ~ 0.7. Overexpression of the protein was induced by adding 0.7 mM isopropyl-β-D-thiogalactopyranoside (IPTG) into the culture. The culture was further incubated at 18 ºC for 15~17 hours under dark condition before harvesting the cells for protein purification.

The following purification processes were conducted under red-light or dark condition. Sonication method was employed to release the target protein from the harvested cell pellet. The sonication supernatant was collected using centrifuge and incubated with FMN on ice for at least 45 min. The protein was purified with column chromatography starting with loading the supernatant onto a Ni-NTA Agarose column for affinity purification of His-tagged protein. The column was washed with 50 mM imidazole buffer and His-tagged $OaPAC_{BLUF}$ was eluted with 250 mM imidazole buffer. The high salt containing imidazole elusion buffer was then exchanged into storage buffer (50 mM Na_2HPO_4/NaH_2PO_4 pH 8.0, 100 mM NaCl, 2 mM DTT, 5% Glycerol) using an SDG-25 gel-filtration chromatography column according to standard laboratory procedure. The purified protein was stored at -80 ºC after quick-frozen with liquid nitrogen.

All of the protein samples were diluted to 200~300 μM before transient absorption experiments. The storage buffer was exchanged into Na_2HPO_4/NaH_2PO_4 pH = 8.0 buffer with SDG-25 column chromatography. Some of the protein samples were prepared as dried powder by lyophilization. They were solubilized in pH = 8.0 H_2O buffer and filtered with a 0.45 μm syringe filter before transient absorption (TA) experiment. For D_2O experiments, the samples were prepared by exchanging the pH = 8.0 H_2O buffer into pD = 8.5 D_2O buffer by incubation (5 hrs) and lyophilization for three cycles, where the protein was incubated for at least 5 hours in each exchange cycle to ensure complete H/D exchange.

Steady-State Spectroscopy

Steady-state UV/Vis spectra of $OaPAC_{BLUF}$ mutants were analyzed with a UV/Vis spectrometer (UV-2600, Shimadzu, Japan) under dark condition. All samples were measured with in a 2-mm pathlength cuvette and sample concentrations were controlled at 200~300 μM. Because the signaling state of $OaPAC_{BLUF}$ WT only persists for seconds, preventing the recording of the red-shifted UV/Vis spectrum using a steady-state UV/Vis spectrometer (UV-2600, Shimadzu, Japan), the static red-shifted UV/Vis spectrum of WT (400 μM) was measured with the commercial TA spectrometer (Helios Fire, Ultrafast Systems, USA) after being exposed to a 450-nm blue light continuously from laser diode (15 mW) as reported in our previous work (1). The pump beam which was employed in the TA experiments was blocked as the time-dependent measurement function is not required in steady-state spectroscopy.

Transient Absorption (TA) Spectroscopy

The TA system was based on a Titanium/Sapphire femtosecond laser system (Solstice ACE, Spectral Physics, USA) with 1 kHz repetition rate and output of ~100-fs pulse centered at 800 nm. For the pump beam, part of the 800-nm pulse was directed into an optical parametric amplifier (TOPAS-Prime, Spectra Physics, USA) to generate 480-nm pump pulse. The pump pulse was attenuated to 0.1 mW before reaching the protein sample cell. Part of the 800-nm pulse feeds a commercial transient absorption spectrometer (Helios Fire, Ultrafast Systems, USA) which includes the white light continuum generation systems and a detector system. The visible continuum generation stage with Sapphire crystal and UV continuum generation stage with CaF_2 crystal were both employed in this work to probe from the UV to visible region. The build-in delay line in the TA spectrometer has a time window up to 7 ns. A half-waveplate was used to adjust the relative polarization between pump pulse and probe pulse to magic angle (54.7°). Sample (200~300 μM) refreshing was achieved with a stir-bar in the 2-mm pathlength cuvette. Because the signaling state of $OaPAC_{BLUF}$ W90F only persists for 12 seconds (Figure S2), there is almost no light-state species accumulated during the measurement, which is double-checked with a control experiment using a flow cell. Static UV/Vis absorption measurements were taken during the laser experiment to monitor the sample condition, ensuring that the samples were replaced if photo-damaged.

A Step-by-step Tutorial on Data Analysis

In order to obtain the rate constant for the branching pathway (τ_{ISC}) of FMN^* decay, an ET and PT inert Y6F/W90F mutant was designed and its kinetic was analyzed by fitting the transient absorption data globally using a sequential model describing the process of the excited oxidized flavin (FMN^*) decaying into the FMN triplet state (^{3}FMN). The evolution associated difference spectra (EADS) are obtained and shown in Fig. S4. Individual kinetic at 760 nm was also fitted with the sequential model where the fitting results are shown in Fig. S4*C* exhibiting the kinetic traces of the two species involved. From this analysis, τ_{ISC} is determined to be 2.8 ns and will be fixed in the target analysis for the other three mutants.

In order to describe the multi-phasic kinetics observed in 760 nm of W90F (referred to as WT in the manuscript), a stretched parameter β is used. And the expression for reaction rate, $\frac{1}{\tau_i}$, in the rate equation is substituted by $\beta_i \frac{t^{\beta_i - 1}}{\tau_i{}^{\beta_i}}$ for further data analysis. (2, 3) The kinetics solved from differential equations below were convoluted with the instrument response function (IRF, ~100 fs) during the fitting. All the target analyses described in the following paragraphs were conducted using a script written in MATLAB. Kinetic at 760 nm was chosen to analyze the decay of FMN^* because the signals above 720 nm are contributed by ^{3}FMN and FMN^*only. Assuming that the total concentration of the excited oxidized flavin (FMN^*) is n_0 initially after excitation, the 760 nm kinetics was fitted as a summation of FMN^* and ^{3}FMN kinetics using the equations [S1-2] below where τ_{ISC} is fixed as 2.8 ns. As a result, we obtain the pure kinetic trace of FMN^* where τ_1 and β_1 are determined to be 172 ps and 0.5, respectively.

$$\frac{d}{dt}[\mathrm{FMN}^*(t)] = -\beta_1 \frac{t^{\beta_1 - 1}}{\tau_1 \beta_1}[\mathrm{FMN}^*(t)] - \frac{1}{\tau_{ISC}}[\mathrm{FMN}^*(t)] \quad [S1]$$

$$\frac{d}{dt}[^3\mathrm{FMN}(t)] = \frac{1}{\tau_{ISC}}[\mathrm{FMN}^*(t)] \quad [S2]$$

The TA data of WT was globally analyzed using the conventional sequential model (EADS) to obtain the spectrum of FMN* which is referred as Spectrum1 (Fig. S18). Spectrum1 contains the typical characteristics of FMN* TA absorption. Considering the decay of FMN* (<τ> = 344 ps) is not in sub-picosecond time scale, Spectrum1 is a sufficient approximation of a pure FMN* spectrum.

The FMN* component was then subtracted from the raw WT TA data matrix using a method inspired by the Tahara's group (4, 5) where the FMN* component is treated as a matrix as shown in equation [S3]. $[\mathrm{Spectrum1}]_{m\times 1}$ is the spectrum of the pure FMN* and $[\mathrm{Kin1}]_{1\times n}$ is the extracted FMN* decay kinetic trace obtained as described above using equations [S1-2]. A1 is the weight of the spectra and kinetic vector. The FMN* component subtracted matrix is obtained by subtracting $[\mathrm{FMN}^*]_{m\times n}$ from the raw WT TA matrix and the result of this subtraction is shown in main text Fig. 2*F*. This is an important step providing key information that the first step proceeds via PCET and forms FMNH· as the intermediate species. This also indicates that the τ_1 and β_1 obtained above describe the decay of FMN* via a forward PCET process. This FMN* subtracted matrix also shows that the FMNH· decays and forms the red shifted state ($\mathrm{FMN_{red}}$).

$$[\mathrm{FMN}^*]_{m\times n} = \mathrm{A1} \cdot [\mathrm{Spectrum1}]_{m\times 1} \cdot [\mathrm{Kin1}]_{1\times n} \quad [S3]$$

In order to obtain τ_2 and β_2 to describe the reverse PCET for the FMNH· decay and the formation of $\mathrm{FMN_{red}}$, kinetics at 500 nm and 550 nm were chosen to be fitted simultaneously along with 760 nm kinetics. Where the 760 nm kinetics was fitted using equations [S1-2] as described above. The 550 nm kinetics was fitted with equations [S1-2, 4] as it also has absorption from FMNH· in this wavelength. 500 nm was fitted with equations [S1-2, 4-5] as $\mathrm{FMN_{red}}$ has a larger absorption here. τ_1, β_1, and τ_{ISC} were fixed to be 172 ps, 0.5, and 2.8 ns, respectively during the global fitting of the selected kinetics at the three wavelengths. Note that the amplitude of ^{3}FMN component was fixed according to the EADS results of Y6F/W90F mutant.

$$\frac{d}{dt}[\mathrm{FMNH}^{\cdot}(t)] = \beta_1 \frac{t^{\beta_1 - 1}}{\tau_1 \beta_1}[\mathrm{FMN}^*(t)] - \beta_2 \frac{t^{\beta_2 - 1}}{\tau_2 \beta_2}[\mathrm{FMNH}^{\cdot}(t)] \quad [S4]$$

$$\frac{d}{dt}[\mathrm{FNN_{red}}(t)] = \beta_2 \frac{t^{\beta_2 - 1}}{\tau_2 \beta_2}[\mathrm{FMNH}^{\cdot}(t)] \quad [S5]$$

To deconvolute the SADS spectra of all involving species (FMN^*, $FMNH^{\cdot}$, FMN_{red}, ^3FMN) in WT, τ_1, β_1, τ_2, β_2, and τ_{ISC} obtained from above were fixed and the full WT matrix was analyzed using equations [S6-9]. The $A4 \cdot [SADS4]_{m\times1}$ describing ^3FMN SADS was fixed according to Y6F/W90F EADS results. The resulting pure species spectra are $Ai \cdot [SADSi]_{m\times1}$ and kinetic traces are $[Kini]_{1\times n}$ where i denotes each species as indicated in equations [S6-9]. The model described by equations [S1-2, 4-5] is shown in the main text Fig. 3F, the resulting pure species SADS spectra and kinetic traces are shown in the main text Fig. 4. The residual matrix of this target analysis is shown in Fig. S19 demonstrating the goodness of this fit. The same procedures described in this section were applied for the D_2O case and the resulting parameters are listed in Table 1 in the main text.

$$[FMN^*]_{m\times n} = A1 \cdot [SADS1]_{m\times1} \cdot [Kin1]_{1\times n} \quad [S6]$$

$$[FMNH^{\cdot}]_{m\times n} = A2 \cdot [SADS2]_{m\times1} \cdot [Kin2]_{1\times n} \quad [S7]$$

$$[FMN_{red}]_{m\times n} = A3 \cdot [SADS3]_{m\times1} \cdot [Kin3]_{1\times n} \quad [S8]$$

$$[^3FMN]_{m\times n} = A4 \cdot [SADS4]_{m\times1} \cdot [Kin4]_{1\times n} \quad [S9]$$

The same analysis procedures described for WT were applied for Q48A/W90F (referred to as Q48A in the manuscript). There are a few differences to note compared to the WT analysis, Q48A does not form FMN_{red} and its target analysis model (main text, Fig. 3*E*) is described with equations [S10-12]. τ_1 and β_1 for forward PCET process were obtained by fitting the 760 nm kinetic trace which is the same method as used in the analysis of WT. The rPCET τ_2 and β_2 were obtained from simultaneous fitting of 620 nm, 520 nm, 445 nm, and 380 nm using equations [S10-12]. In Q48A, ^3FMN has a distinct kinetic trace profile and thus, the ^3FMN amplitude in Q48A was not fixed during the target analysis. The resulting SADS and kinetic traces for Q48A are shown in Fig. S9 whereas the residual matrix is shown in Fig. S19.

$$\frac{d}{dt}[FMN^*(t)] = -\beta_1 \frac{t^{\beta_1-1}}{{\tau_1}^{\beta_1}}[FMN^*(t)] - \frac{1}{\tau_{ISC}}[FMN^*(t)] \quad [S10]$$

$$\frac{d}{dt}[^3FMN(t)] = \frac{1}{\tau_{ISC}}[FMN^*(t)] \quad [S11]$$

$$\frac{d}{dt}[FMNH^{\cdot}(t)] = \beta_1 \frac{t^{\beta_1-1}}{{\tau_1}^{\beta_1}}[FMN^*(t)] - \beta_2 \frac{t^{\beta_2-1}}{{\tau_2}^{\beta_2}}[FMNH^{\cdot}(t)] \quad [S12]$$

For Q48E/W90F (referred to as Q48E in the manuscript), the same analysis procedures described above for WT were applied. There are a few differences to be noted in Q48E target analysis processes. The $FMNH^{\cdot}$ species formed in Q48E does not decay in our time window, thus its model as shown in main text Fig. 3*D* is described with equations [S13-15] without the τ_2 and β_2, excluding a reverse PCET process. Similar to WT

and Q48A, the forward PCET parameters (τ_1 and β_1) were obtained from fitting the 760 nm kinetic using equations [S13-14]. As the kinetic trace describing the formation of $FMNH^{\cdot}$ (equation S15) is not easily distinguished from the kinetic trace for the formation of ^{3}FMN, the amplitude of ^{3}FMN, $A4 \cdot [SADS4]_{m\times 1}$, in Q48E was fixed during the target analysis process using the EADS results of Y6F/Q48F which is similar to the approach used in WT target analysis. The resulting SADS and kinetic traces for Q48E are shown in Fig. S8 and its' residual matrix is shown in Fig. S18.

$$\frac{d}{dt}[\mathrm{FMN}^*(t)] = -\beta_1 \frac{t^{\beta_1-1}}{{\tau_1}^{\beta_1}}[\mathrm{FMN}^*(t)] - \frac{1}{\tau_{ISC}}[\mathrm{FMN}^*(t)] \quad [S13]$$

$$\frac{d}{dt}[^3\mathrm{FMN}(t)] = \frac{1}{\tau_{ISC}}[\mathrm{FMN}^*(t)] \quad [S14]$$

$$\frac{d}{dt}[\mathrm{FMNH}^{\cdot}(t)] = \beta_1 \frac{t^{\beta_1-1}}{{\tau_1}^{\beta_1}}[\mathrm{FMN}^*(t)] \quad [S15]$$

Molecular Dynamics Simulations

The MD simulations were performed using Groningen Machine for Chemical Simulations (GROMACS) software package. (6–8) Amber03 force field was employed during the simulations. The force field of the FMN chromophore is generated by AmberTools21. The initial protein structure coordinates were obtained from existing WT OaPAC crystal structure (PDB: 4YUT) where the mutations were constructed with the PyMOL software for Q48E, Q48A and WT to generate the initial structure for the MD simulations. The water mode was TIP3P. The Glu residues in all three proteins were deprotonated except for the Glu48 in Q48E mutant according the transient infrared (TRIR) results of the Q63E mutant of AppA (9, 10). A cuboid box was created and the distance between the box boundary and protein was set to be 1 nm. The protein was solvated by water molecules in the box. System neutralization was conducted by adding Na^+ counterions. Energy minimization (tolerance of 10 kJ•mol^{-1}, maximum steps of 50000) was applied to ensure that the system has no steric clashes or inappropriate geometry. System pre-equilibration was conducted to equilibrate the solvent and ions under two phases, NVT ensemble (100 ps, 2 fs step size, 300 K) to stabilize the temperature of the system and NPT ensemble (100 ps, 2 fs step size, 300 K, 1 bar) to stabilize the pressure of the system. Finally, a 200-ns MD simulation trajectory (2-fs step size) was obtained after the pre-equilibration processes at 300 K and 1 bar to mimic the experimental condition.

Table S1. Multiexponential fit of 760 nm kinetics of the three mutants in H_2O and D_2O using $y(t) = \sum A_i e^{-t/\tau} + A_{\text{offset}}$.

	A_1 (%)	τ_1 (ps)	A_2 (%)	τ_2 (ps)	A_3 (%)	τ_3 (ps)	A_{offset} (%)
WT (H_2O)	16.6	2.97	38.4	72	41.3	456	3.7
WT (D_2O)	21.8	2.44	27.8	62	43	537	7.4
Q48A (H_2O)	32.9	14	59.5	110	7.6	841	0
Q48A (D_2O)	11	6.9	48	62	38.5	370	2.5
Q48E (H_2O)	35.0	44	62.5	273			2.5
Q48E (D_2O)	46.3	129	47.5	688			6.2

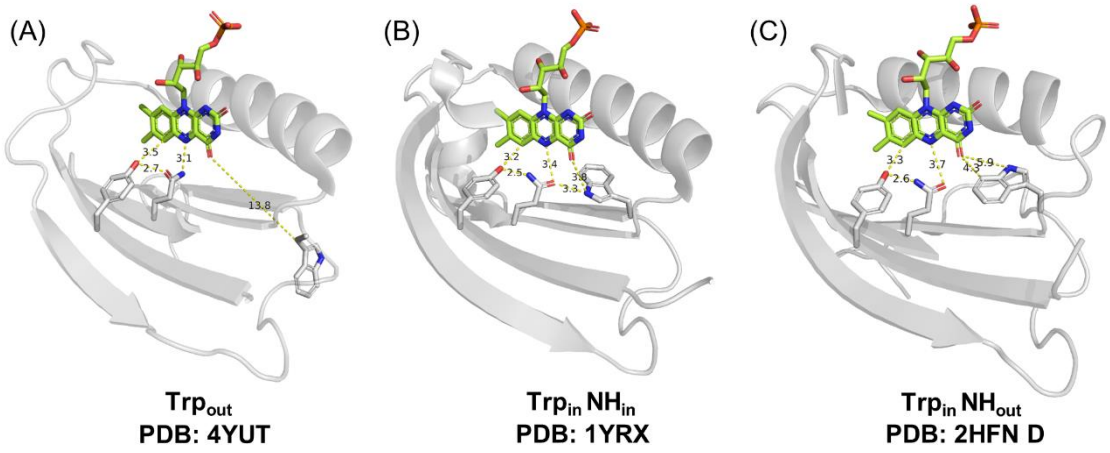

Fig. S1. Structures of the BLUF domain illustrating the (*A*) Trp_{out} (PDB entry: 4YUT), (*B*) Trp_{in}-NH_{in} (PDB entry: 1YRX) and (*C*) Trp_{in}-NH_{out} (PDB entry: 2HFN) conformations.

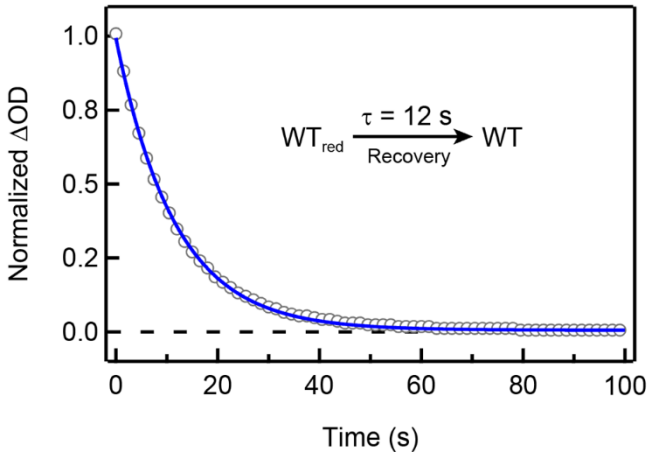

Fig. S2. Dark state recovery kinetics of WT. The kinetic trace was obtained by monitoring the absorbance change at 510 nm. The dark state recovery lifetime was determined by fitting the curve with a single exponential function.

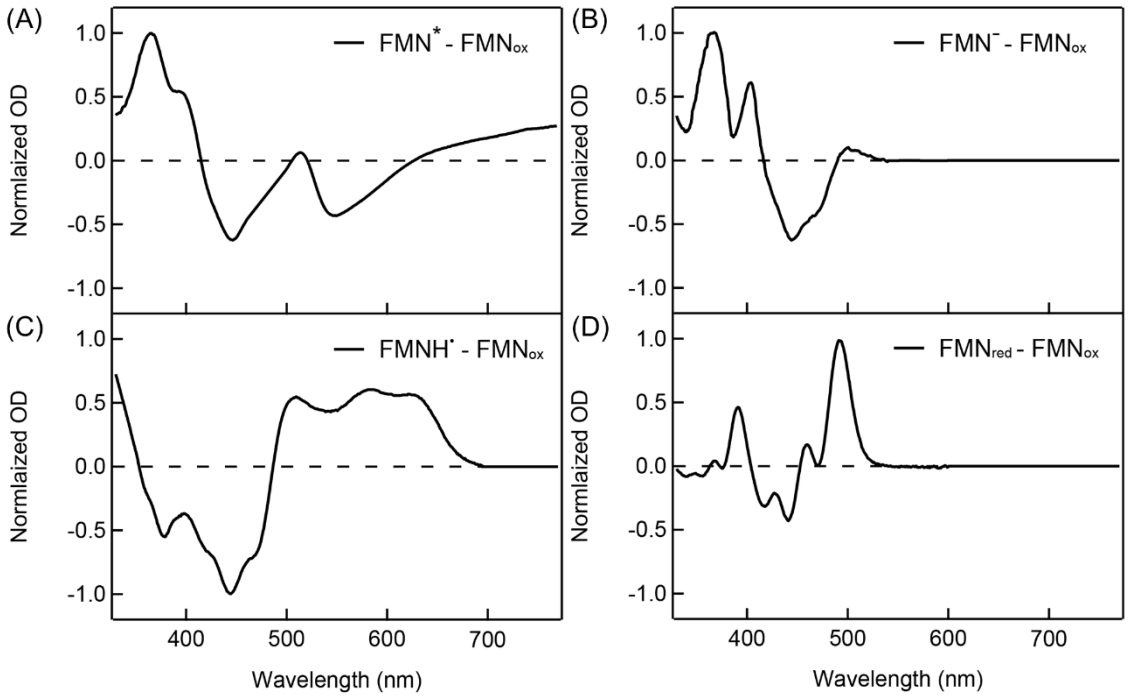

Fig. S3. The UV/Vis difference static absorption spectra of FMN^* (*A*), $FMN^{\cdot-}$ (*B*), $FMNH^{\cdot}$ (*C*) and FMN_{red} (*D*), with respect to FMN_{ox}. The FMN^* is obtained from $OaPAC_{BLUF}$ Y6W/W90F target analysis results. (1) The difference absorption spectra of $FMN^{\cdot-}$ and $FMNH^{\cdot}$ are obtained from the references.(11, 12) The difference absorption spectrum of FMN_{red} is obtained by measuring the dark and red-shifted UV/Vis spectra of WT. This will be quite useful in interpretation of the TA spectra by showing the relevant species' characteristic absorptions.

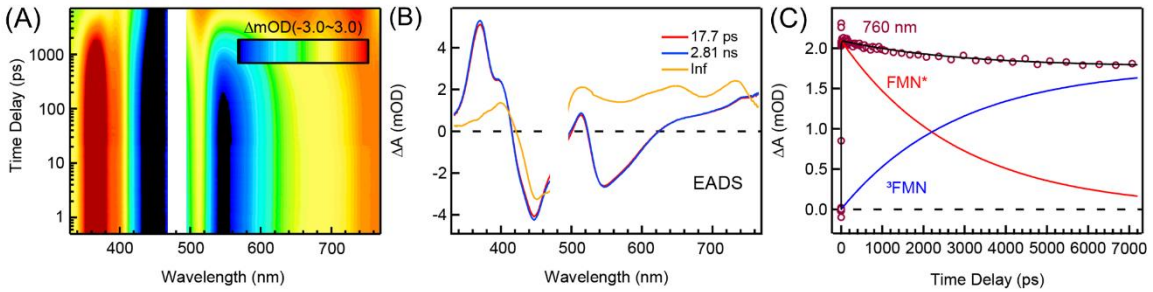

Fig. S4. (*A*) The original transient absorption 2D spectra of Y6F/W90F in H_2O. (*B*) The EADS spectra extracted from the global fitting results where the line in yellow shows the spectra feature of ^{3}FMN. (*C*) The kinetics decomposition of the dynamics at 760 nm for Y6F/W90F in H_2O.

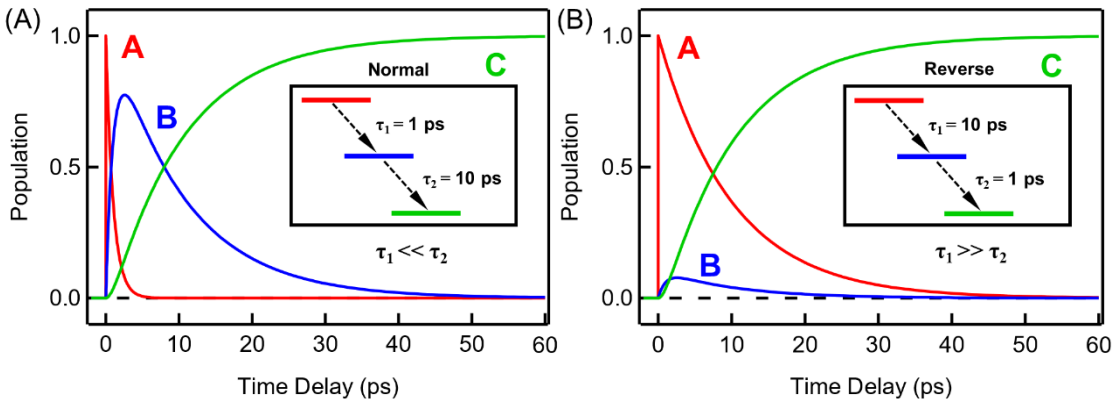

Fig. S5. Illustration of the difference of the intermediate species' population in a normal kinetics (*A*) versus a inverted kinetics (*B*) model. Species A, B and C represent the reactant, the intermediate and the product, respectively. Note that in the inverted kinetics model, the decay of B matches with τ_1 and the rise τ_2. The profile of B in the inverted kinetics is the same as that in the normal kinetics, only with the feature of a much smaller population, which is the case in WT in our work.

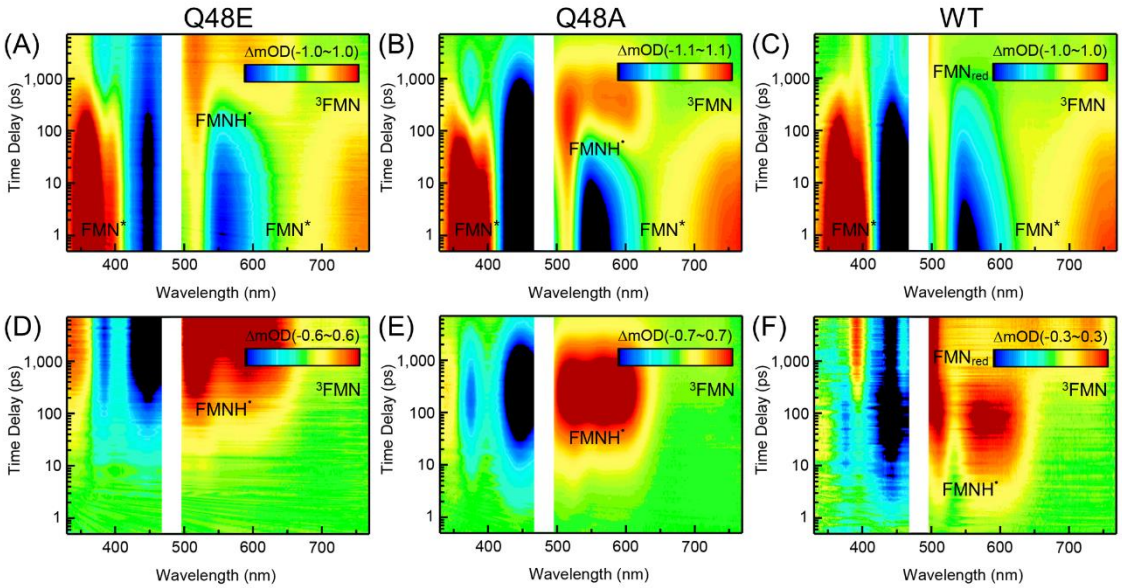

Fig. S6. (*A-C*) Original transient absorption 2D spectra of Q48E, Q48A and WT in D_2O. (*D-F*) The corresponding transient absorption 2D spectra of Q48E, Q48A and WT after subtracting the contribution of FMN^* from the original data in D_2O. The transient species of FMN^*, $FMNH^{\cdot}$, ^3FMN and FMN_{red} are denoted in the 2D contour maps.

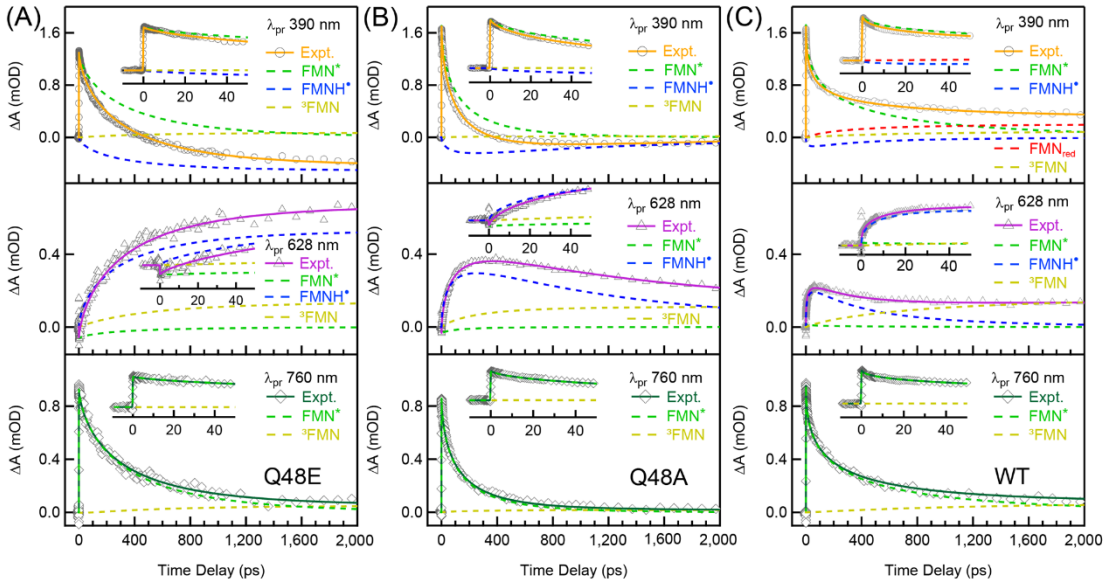

Fig. S7. (*A-C*) Transient absorption kinetics traces of Q48E, Q48A and WT, respectively in D_2O cut from the 2D contour map at selected wavelengths (760 nm, 628 nm and 390 nm), with the decomposed dynamics of the reactant (FMN^*), the intermediate ($FMNH^\bullet$), and the products (FMN_{red} and ^3FMN). Raw data are represented with symbols and the fitted kinetics are represented with straight lines. The kinetics of the given species are shown in colored dash lines.

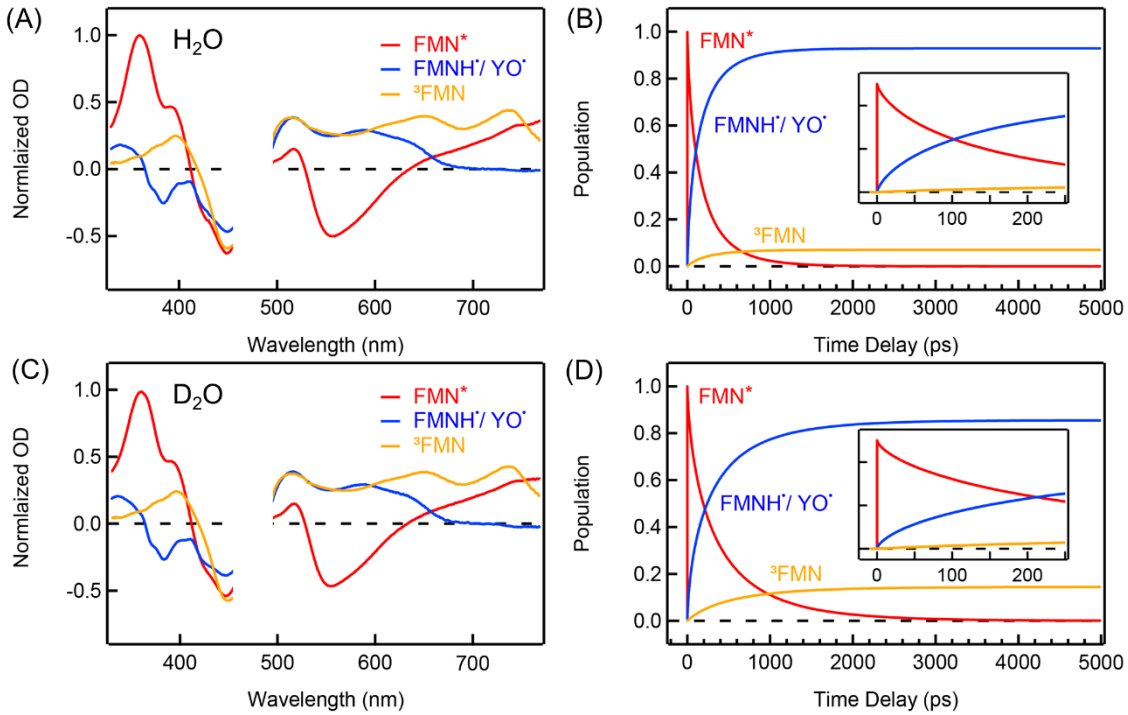

Fig. S8. SADS of Q48E in H_2O (*A*) and D_2O (*C*) condition. The corresponding kinetic traces are shown in *B* and *D*. The population evolutions of FMN^*, $FMNH^{\cdot}$ and ^3FMN are represented by the red, blue and yellow solid lines.

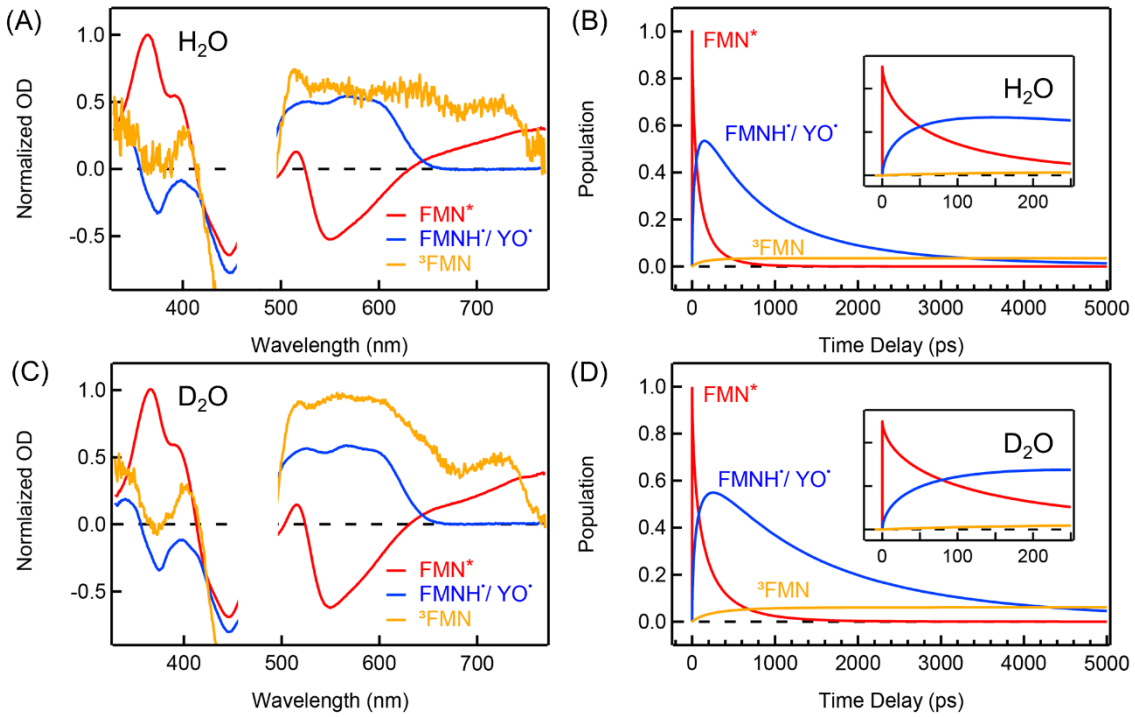

Fig. S9. SADS of Q48A in H_2O (*A*) and D_2O (*C*) condition. The corresponding kinetic trace diagrams are shown in *B* and *D*. The population evolutions of FMN^*, $FMNH^{\cdot}$ and ^3FMN are represented by the red, blue and yellow solid lines. The ^3FMN SADS is not fixed as it has distinguishable kinetic trace from those of others.

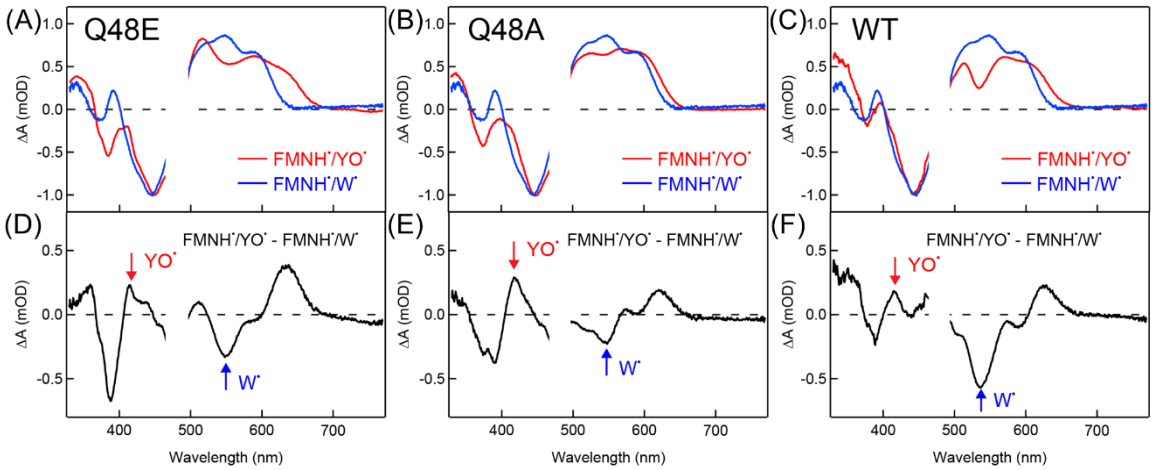

Fig. S10. (*A-C*) The normalized SADS of FMNH˙/YO˙ (red line) in mutant Q48E, Q48A and WT. The normalized SADS of FMNH˙/W˙ (blue line) extracted from the global fitting results of Y6W/W90F.(1) (*D-F*) The difference between the corresponding FMNH˙/YO˙ of mutant Q48E, Q48A and WT to the FMNH˙/W˙ of Y6W/W90F. The red arrows in the figure denote the signal of YO˙ and the blue arrows the signal of W˙.

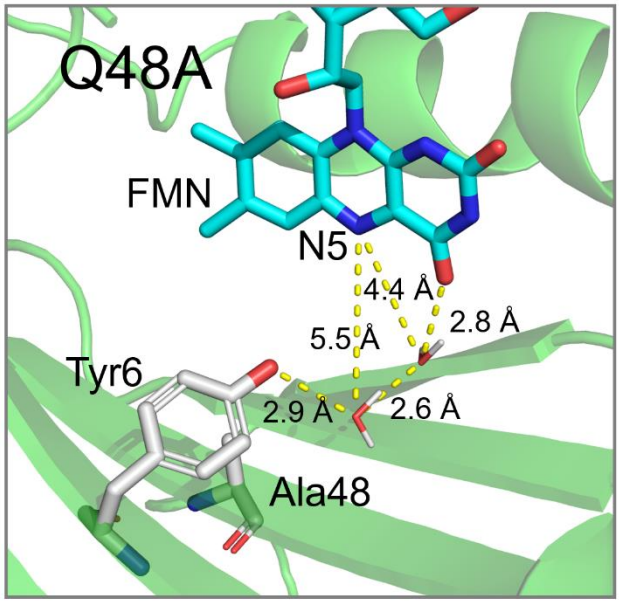

Fig. S11. The representative snapshot for the minor population in Fig. 5 where the bound water molecules in Q48A form H-bond bridges between TyrO and the C4=O of FMN.

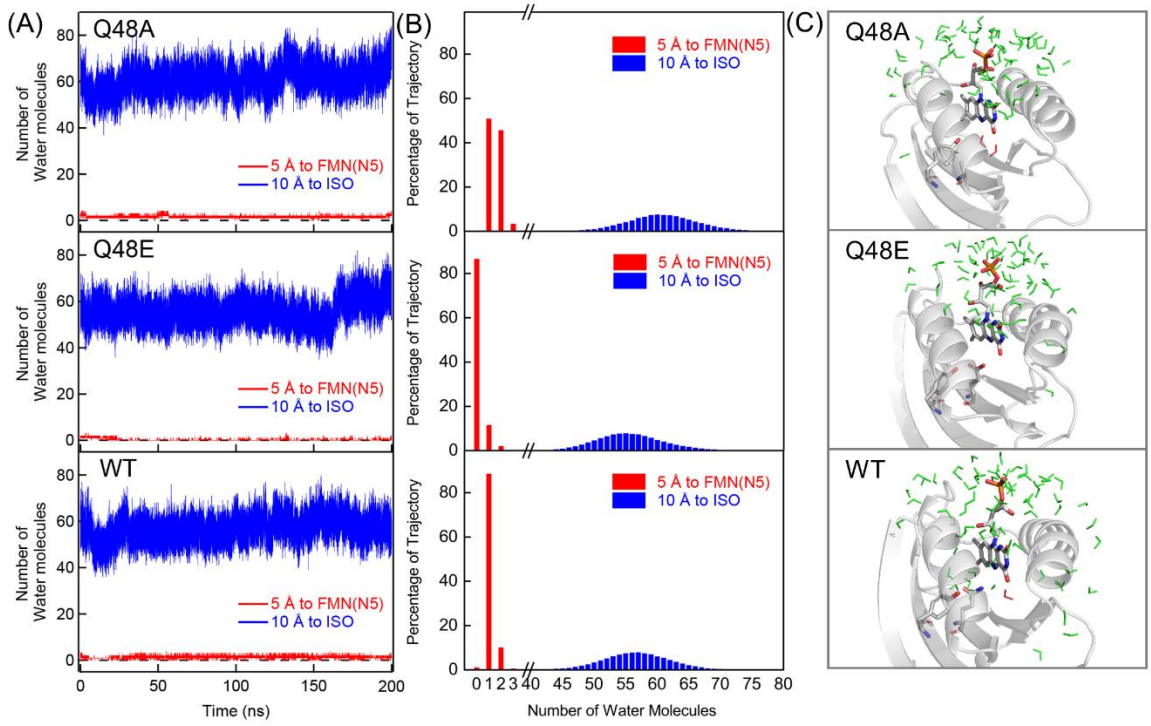

Fig. S12. (*A*) 200 nanosecond snapshots of MD simulation on Q48A, Q48E and WT. The total water molecules at a distance of < 5 Å to the N5 of FMN (red) and < 10 Å to the isoalloxazine (ISO) ring of FMN (blue). (*B*) The corresponding distribution of the water molecules numbers surround the N5 (< 5 Å) and isoalloxazine ring (< 10 Å) of FMN. The water molecules within 5 Å are mostly structural water in the cavity. The dynamics water molecules within 10 Å are mostly around the charged phosphate group of FMN. (*C*) The representative snapshot for the water molucules surround the N5 and isoalloxazine ring of FMN in Q48A, Q48E and WT. The water molecules are displayed in red color (< 5 Å, structural water) and green color (< 10 Å, dynamics water molecules) for comparision.

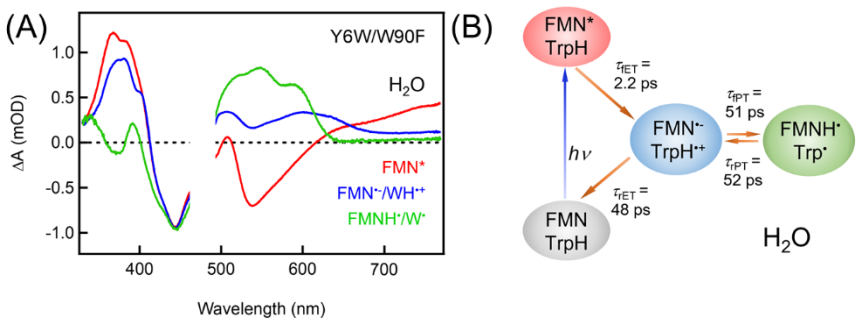

Fig. S13. (*A*) The reported SADS spectra of Y6W/W90F mutant in H_2O. (*B*) The reported kinetic model of Y6W/W90F. (1)

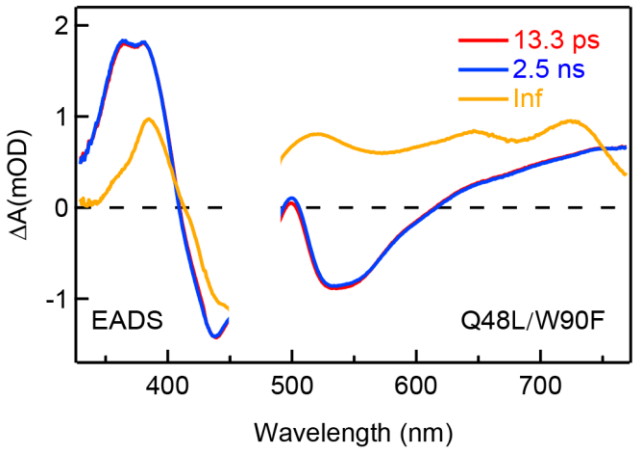

Fig. S14. The EADS spectra of Q48L/W90F extracted from the global fitting results where the line in yellow shows the spectra feature of ^{3}FMN. The 13.3 ps denotes the solvation time and the 2.5 ns is the timescale for intersystem crossing.

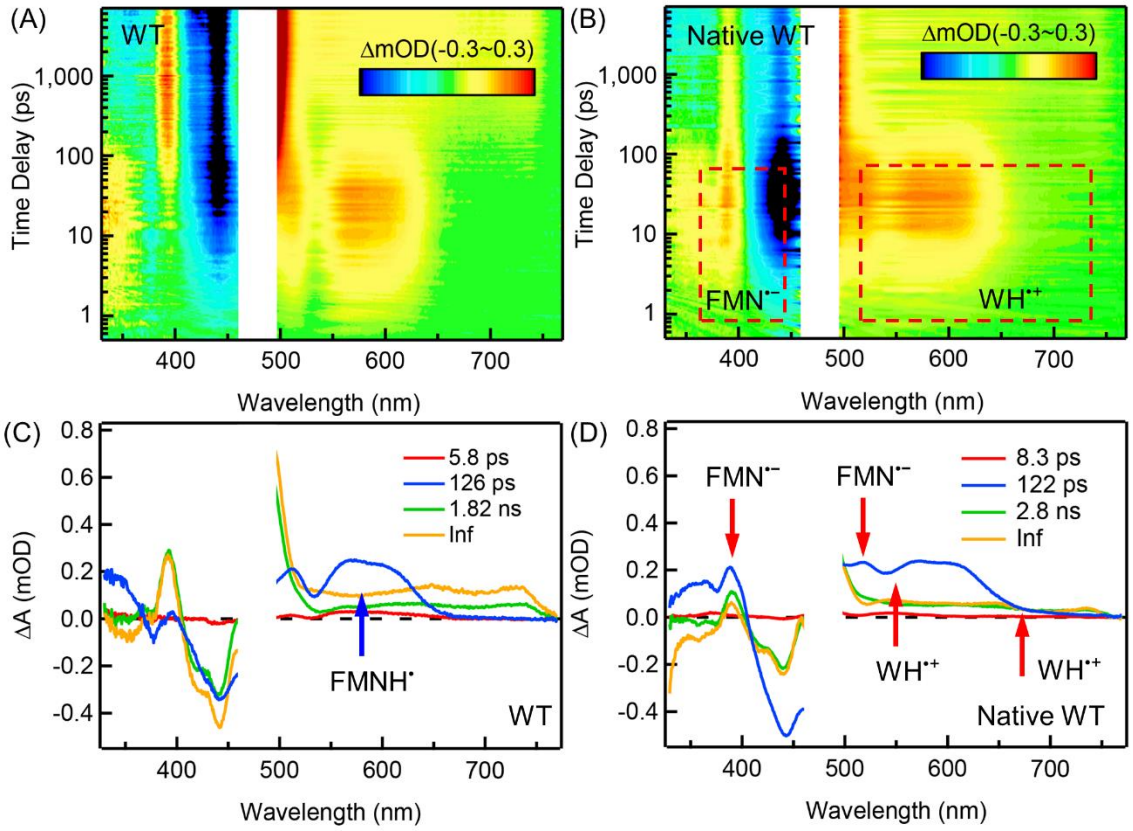

Fig. S15. The transient absorption 2D contour map of W90F (WT in the manuscript) (*A*) and the native WT (*B*) after subtracting the contribution of FMN^{*}. The red square dash denotes the signal of $FMN^{\bullet -}$ (see Fig. S3*B*) and $WH^{\bullet +}$ observed in native WT but is absent in WT. (*C-D*) The corresponding EADS. The arrow denotes the transient signal of $FMN^{\bullet -}$, $WH^{\bullet +}$ and $FMNH^{\bullet}$ in the EADS.

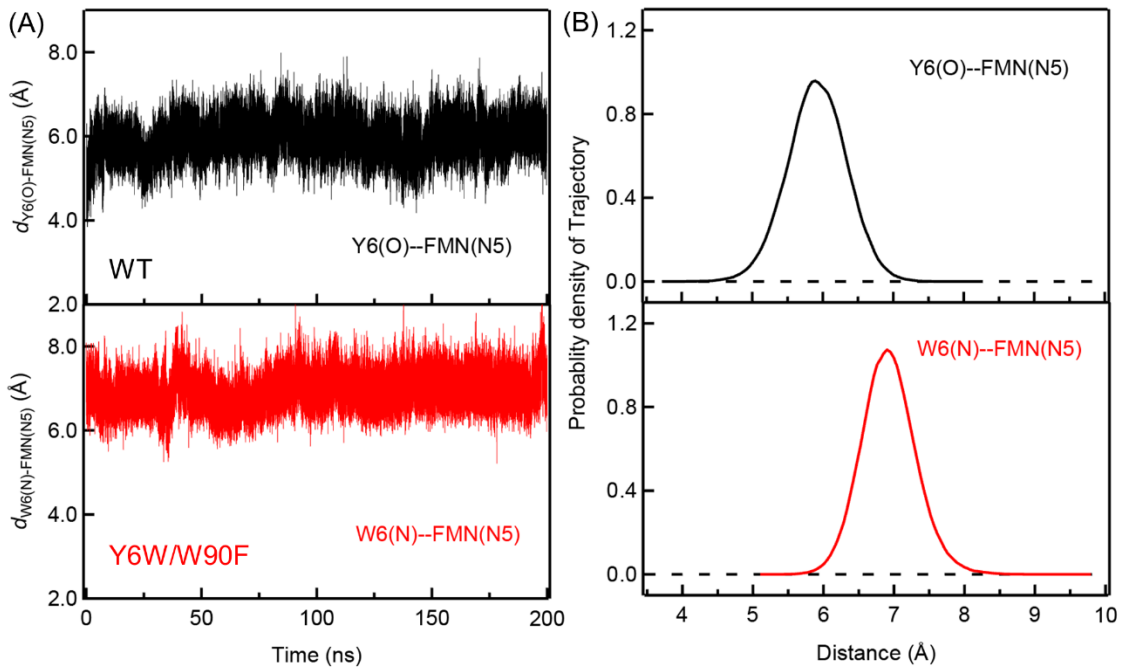

Fig. S16. (*A*) The time evolution of simulated distance between the O of Tyr6 to N5 of FMN in WT and N of Trp6 to N5 of FMN in Y6W/W90F. (*B*) Distribution of the simulated distances between two atoms calculated with MD simulation in 200 ns.

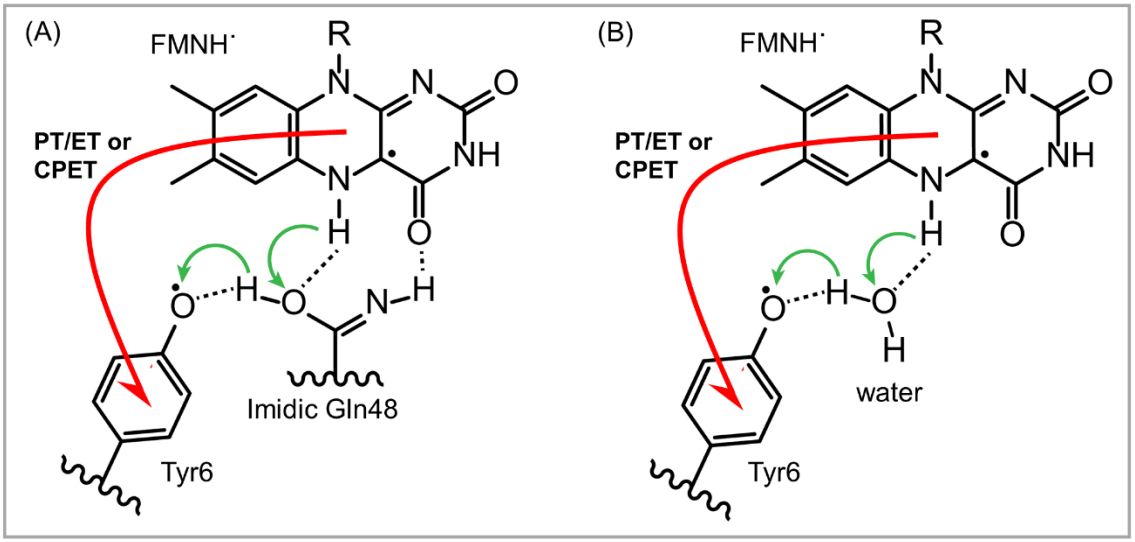

Fig. S17. (*A*) Proposed reverse PCET mechanism by the Park group (13) for WT. (*B*) Proposed reverse PCET mechanism for Q48A in this work. Note the similarity of the pathways in the two cases. Flows of the electrons and protons are denoted by the red and green arrows, respectively.

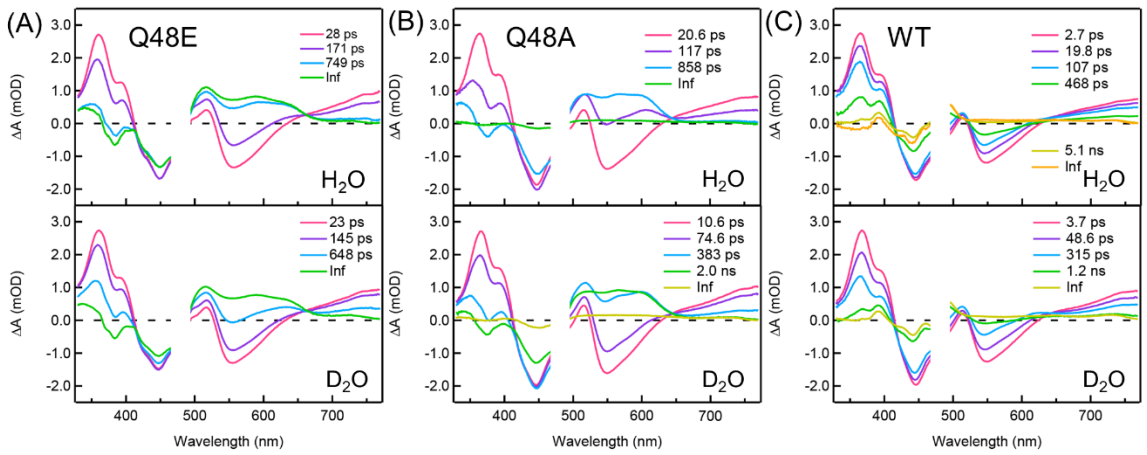

Fig. S18. The evolution associated spectra (EADS) of Q48E (*A*), Q48A (*B*) and WT (*C*) in H_2O and D_2O conditions.

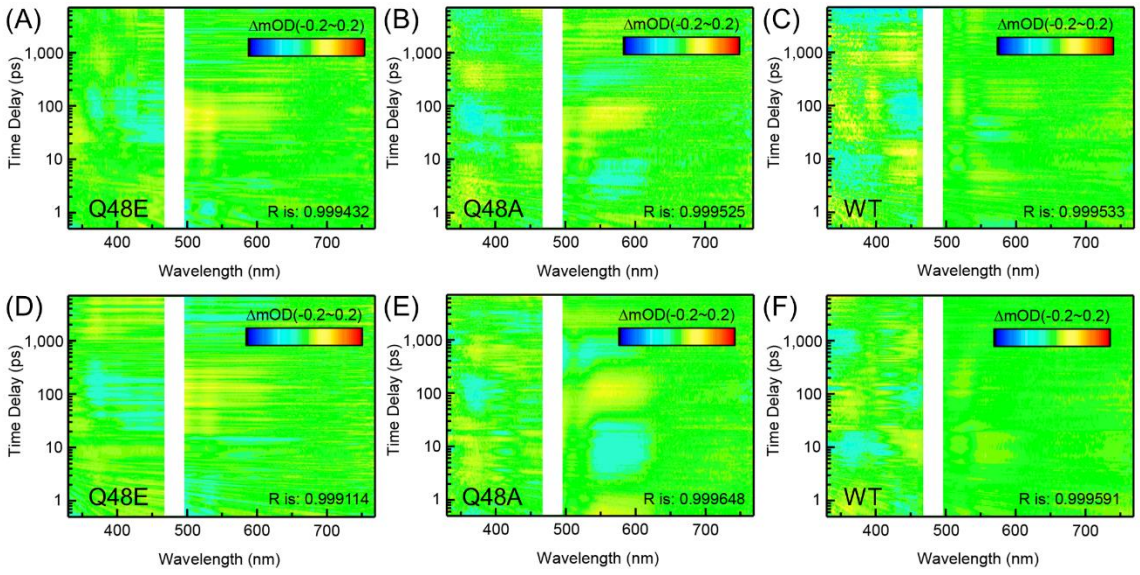

Fig. S19. (*A-C*) The SADS residual matrices of Q48E, Q48A and WT in H_2O condition. (*D-F*) The corresponding residual matrices in D_2O condition. R is the correlation coefficient of the data and fitting results.

SI References

1. X.-W. Kang *et al.*, Direct observation of ultrafast proton rocking in the BLUF domain. *Angew. Chem. Int. Ed.* e202114423 (2022).
2. T.-F. He *et al.*, Femtosecond dynamics of short-range protein electron transfer in flavodoxin. *Biochemistry* **52**, 9120–9128 (2013).
3. M. Kundu, T.-F. He, Y. Lu, L. Wang, D. Zhong, Short-range electron transfer in reduced flavodoxin: ultrafast nonequilibrium dynamics coupled with protein fluctuations. *J. Phys. Chem. Lett.* **9**, 2782–2790 (2018).
4. T. Fujisawa, S. Masuda, S. Takeuchi, T. Tahara, Femtosecond time-resolved absorption study of signaling state of a BLUF protein PixD from the cyanobacterium *Synechocystis*: hydrogen-bond rearrangement completes during forward proton-coupled electron transfer. *J. Phys. Chem. B* **125**, 12154–12165 (2021).
5. T. Fujisawa, S. Takeuchi, S. Masuda, T. Tahara, Signaling-state formation mechanism of a BLUF protein PapB from the purple bacterium *Rhodopseudomonas palustris* studied by femtosecond time-resolved absorption spectroscopy. *J. Phys. Chem. B* **118**, 14761–14773 (2014).
6. B. Hess, C. Kutzner, D. van der Spoel, E. Lindahl, GROMACS 4: Algorithms for highly efficient, load-balanced, and scalable molecular simulation. *J. Chem. Theory Comput.* **4**, 435–447 (2008).
7. S. Pronk *et al.*, GROMACS 4.5: a high-throughput and highly parallel open source molecular simulation toolkit. *Bioinformatics* **29**, 845–854 (2013).
8. H. J. C. Berendsen, D. van der Spoel, R. van Drunen, GROMACS: A message-passing parallel molecular dynamics implementation. *Comput. Phys. Commun.* **91**, 43–56 (1995).
9. A. Lukacs, P. J. Tonge, S. R. Meech, Photophysics of the blue light using flavin domain. *Acc. Chem. Res.* **55**, 402–414 (2022).
10. A. Lukacs *et al.*, Radical formation in the photoactivated adenylate cyclase OaPAC Revealed by ultrafast spectroscopy. *Biophys. J.* **118**, 608a (2020).
11. M. Zhang, L. Wang, D. Zhong, Photolyase: dynamics and electron-transfer mechanisms of DNA repair. *Arch. Biochem. Biophys.* **632**, 158–174 (2017).
12. E. Schleicher *et al.*, Electron nuclear double resonance differentiates complementary roles for active site histidines in (6-4) photolyase. *J. Biol. Chem.* **282**, 4738–4747 (2007).
13. M. Ohki *et al.*, Molecular mechanism of photoactivation of a light-regulated adenylate cyclase. *Proc. Natl. Acad. Sci. U. S. A.* **114**, 8562–8567 (2017).